Application of the moist vorticity vector in the analysis of a heavy rainfall event in North China*

Zhao Yu[1, 2, 3**], Wang Jianguo[4] and Xue Deqiang[2]

(1. Laboratory of Cloud-Precipitation Physics and Severe Storms, Institute of Atmospheric Physics, Chinese Academy of Sciences, Beijing 100029, China; 2. Shandong Provincial Meteorological Observatory, Jinan 250031, China; 3. Graduate University of Chinese Academy of Sciences, Beijing 100039, China; 4. Shandong Provincial Meteorological Bureau, Jinan 250031, China)

Accepted on July 20, 2007

Abstract The moist vorticity vector (MVV), defined as $(\zeta_a \times \nabla q_v)/\rho$ introduced by Gao et al. is used to study a heavy rainfall event in North China. The MVV has zonal, meridional and vertical components in a three-dimensional framework. Analysis of domain-mean and mass-integrated quantities shows that the variation of the vertical component of the MVV closely follows the variation of the cloud hydrometeors with a linear correlation coefficient of 0.95, indicating that the vertical component of the MVV is strongly associated with midlatitude convection. Further analysis shows that the vertical component of the MVV reflects the interaction between the horizontal vorticity and the horizontal specific humidity gradient, which can associate dynamic and thermodynamic processes with cloud microphysical processes. Thus, this study can help to understand how the interaction between circulations and clouds aids the development of convection, and the MVV can be used to trace the development and evolution of heavy rainfall.

Keywords: moist vorticity vector, heavy rainfall, modeling study.

Since potential vorticity (PV, defined as $(\zeta_a \cdot \nabla\theta)/\rho$) was first introduced by Ertel[1], it has been extensively used to study the genesis and evolution of weather systems for several decades[2—9] because of its conservation in a frictionless adiabatic flow and its invertibility in a balanced system. In addition, it has enhanced the understanding of the dominant physical processes responsible for the formation and growth of weather systems. However, PV is not conserved when diabatic heating occurs during the development of convection. Bennetts et al.[10] took into account latent heat and deduced the wet bulb potential vorticity equation. At the beginning of the 1990s, Wu et al.[11] replaced potential temperature with equivalent potential temperature and proved that moist potential vorticity (MPV, defined as $(\zeta_a \cdot \nabla\theta_e)/\rho$) is conserved in moist adiabatic processes. They also proposed the theory of slantwise vorticity development, which has considerable application in analyzing mesoscale rainstorms[12—17]. By using MPV, researchers have successfully revealed some important phenomena and facts[18—22].

However, there are some inconveniences associated with the nature of PV in some kinds of practical applications. Gao et al.[23] demonstrated that dry and moist PV cannot be applied to their analysis of two-dimensional (2-D) simulation data since it could be zero for a 2-D equatorial circulation. For deep convection systems, the orientation of equivalent potential temperature gradient is almost horizontal due to the apparent slant of moist isentropic surfaces; scalar product of the absolute vorticity vector and the equivalent potential temperature gradient is a little weak, which makes analysis with MPV a little difficult. To solve this problem, Gao et al.[23—25] introduced two new vorticity vectors based on the definition of MPV. One is the convective vorticity vector (CVV, defined as $(\zeta_a \times \nabla\theta_e)/\rho$), and the other is the moist vorticity vector (MVV, defined as $(\zeta_a \times \nabla q_v)/\rho$). They applied the two vectors to the study of tropical convective systems by using 2-D and 3-D cloud-resolving models and obtained valuable results, showing that variations of the vertical components of CVV and MVV follow the variation of the sum of the cloud hydrometeor mixing ratios with very high linear correlation coefficients. Their studies showed that the vertical components of CVV and MVV are closely associ-

* Supported by National Natural Science Foundation of China (Grant Nos. 40433007 and 40333034), and the Scientific Research Project of the Shandong Provincial Meteorological Bureau (Grant No. 2006sdqxz18)

** To whom correspondence should be addressed. E-mail: zy0817@126.com

ated with tropical convection.

The CVV and MVV have their unique features that can associate dynamic and thermodynamic processes with cloud microphysical processes in tropical convection. Then a question to be answered is: what is the performance of the CVV and MVV in other regions except in tropics, for example, in the midlatitude region? Cui et al.[26] used the CVV to study the development and movement of meso-scale rainstorms in the Jiang-Huai valley of China and found that the distributions of the vertical component of the CVV match the vertical motions and cloud hydrometeors very well and may be a useful diagnostic tool for midlatitude convection. However, till now, few studies have been devoted to the MVV except for Gao et al[24, 25]. The MVV may also be a useful tool for midlatitude convection. So the questions to be answered are: What does the 3-D MVV look like in the midlatitudes? What is the relationship between the MVV and the rainfall? Is the 3-D MVV, especially its vertical component, useful for the analysis of development and movement of heavy rainfalls in the midlatitudes?

In this study, a heavy rainfall event that occurred in North China on 12—13 August 2004 is simulated by the advanced regional prediction system ARPS model, and the high-resolution output data from the simulation is used to analyze the relation between MVV and deep convection.

1 Moist vorticity vector (MVV)

Gao et al.[24] defined a moist vorticity vector as

$$\boldsymbol{M} = \frac{\zeta_a \times \nabla q_v}{\rho} \tag{1}$$

where $\zeta_a = \nabla \times \boldsymbol{V} + 2\Omega$ is the absolute vorticity, q_v is the specific humidity, and ρ is the moist air density. The MVV in Cartesian coordinates can be expressed by

$$\begin{aligned}\boldsymbol{M} = \frac{1}{\rho}\Bigg[&\left(\zeta_y \frac{\partial q_v}{\partial z} - \zeta_z \frac{\partial q_v}{\partial y}\right)\boldsymbol{i} \\ &+ \left(\zeta_z \frac{\partial q_v}{\partial x} - \zeta_x \frac{\partial q_v}{\partial z}\right)\boldsymbol{j} \\ &+ \left(\zeta_x \frac{\partial q_v}{\partial y} - \zeta_y \frac{\partial q_v}{\partial x}\right)\boldsymbol{k}\Bigg] \\ = {} & M_x\boldsymbol{i} + M_y\boldsymbol{j} + M_z\boldsymbol{k}\end{aligned} \tag{2}$$

Here, $\zeta_x = \frac{\partial w}{\partial y} - \frac{\partial v}{\partial z}$, $\zeta_y = \frac{\partial u}{\partial z} - \frac{\partial w}{\partial x} + f$, $\zeta_z = \frac{\partial v}{\partial x} - \frac{\partial u}{\partial y} + f$, where f is the Coriolis parameter, $f = 2\Omega\sin\varphi$, $\tilde{f} = 2\Omega\cos\varphi$, and φ is latitude.

From (2), the three components of the MVV can be written as

$$\begin{aligned}M_x = \frac{1}{\rho}\Bigg[&\left(\frac{\partial u}{\partial z} - \frac{\partial w}{\partial x} + \tilde{f}\right)\frac{\partial q_v}{\partial z} \\ &- \left(f + \frac{\partial v}{\partial x} - \frac{\partial u}{\partial y}\right)\frac{\partial q_v}{\partial y}\Bigg]\end{aligned} \tag{3a}$$

$$\begin{aligned}M_y = \frac{1}{\rho}\Bigg[&\left(f + \frac{\partial v}{\partial x} - \frac{\partial u}{\partial y}\right)\frac{\partial q_v}{\partial x} \\ &- \left(\frac{\partial w}{\partial y} - \frac{\partial v}{\partial z}\right)\frac{\partial q_v}{\partial z}\Bigg]\end{aligned} \tag{3b}$$

$$\begin{aligned}M_z = \frac{1}{\rho}\Bigg[&\left(\frac{\partial w}{\partial y} - \frac{\partial v}{\partial z}\right)\frac{\partial q_v}{\partial y} \\ &- \left(\frac{\partial u}{\partial z} - \frac{\partial w}{\partial x} + \tilde{f}\right)\frac{\partial q_v}{\partial x}\Bigg] = M_{z1} + M_{z2}\end{aligned} \tag{3c}$$

The MVV has three components: zonal (M_x), meridional (M_y) and vertical (M_z). M_x represents the interaction between meridional vorticity and the vertical gradient of specific humidity, and the covariance between vertical vorticity and the meridional gradient of specific humidity. M_y reflects the covariance between vertical vorticity and the zonal gradient of specific humidity, and the covariance between zonal vorticity and the vertical gradient of specific humidity. M_z is determined by the interaction between the horizontal vorticity and the horizontal specific humidity gradient.

In this study, to better understand the relationship between MVV and midlatitude convection, vertical mass-integrated quantities are calculated.

For any two levels ($z_{k+1} - z_k$), $[x] = \int_{z_k}^{z_{k+1}} \rho x \,\mathrm{d}z = \bar{\rho}\left[\frac{(x)_{z_{k+1}} + (x)_{z_k}}{2}\right](z_{k+1} - z_k)$ is used to calculate mass integration of any variable x, the mass-integrated quantity is accumulated for all levels, and $\bar{\rho}$ is the mean air density.

The components M_x, M_y, M_z and the sum of the cloud hydrometeor mixing ratios (i.e. q_c, q_r, q_i, q_s, q_h, the mixing ratios of cloud water (small cloud droplets), raindrops, cloud ice (small ice crystals), snow and hail, respectively) were calculated by using the simulation data. The mass integration $[M_x]$,

[M_y], [M_z], [MPV], and [$q_c+q_r+q_i+q_s+q_h$] (where [ ] is a mass integration) were calculated from 250 to 20500 m.

2 Overview of the heavy rainfall event

A heavy rainfall event that occurred in North China on 12—13 August 2004, was caused mainly by the interaction between the western Pacific subtropical high and weak cold air. Fig. 1(a) shows that a NE-SW oriented rain belt with three main centers covered most parts of Hebei Province, Shanxi Province, Beijing Municipality, and Tianjin Municipality. The first rainfall center (133.2 mm) was located at Yuanshi (37.75°N, 114.53°E), in the southwest of Hebei Province; the second one (107.2 mm) was in Taigu area (37.41°N, 112.58°E), in the middle of Shanxi Province; and the third one (68.7 mm) was in Tanggu area (39°N, 117.71°E). There are 29 standard rain gauge observations exceeding 50 mm, and five exceeding 100 mm in North China during this event.

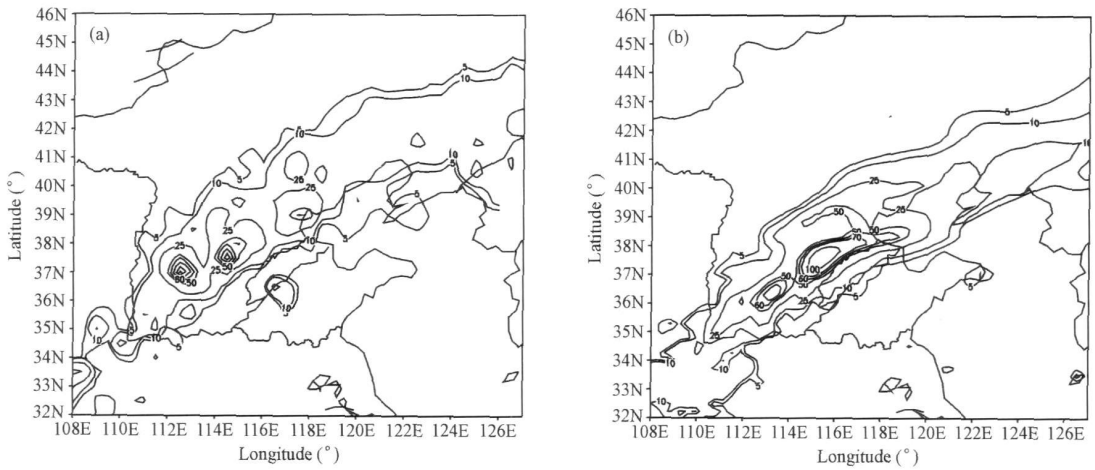

Fig. 1. Observed (a) and simulated (b) rainfall (units: mm) from 00UTC 12 to 00UTC 13 August 2004 (contours: 5, 10, 25, 50, 60, 70, 100 mm).

At 00 UTC 12 August 2004, a short-wave westerly trough with evident cold air advection appeared to the east of Baikal area at 500 hPa level (not shown), and another ENE-WSW oriented westerly trough was passing across northern Inner Mongolia. These two ladder-shaped troughs made cold air continuously intrude into North China. The subtropical high extended westward and northward to cover most parts of Shandong Province because a typhoon was located just over the open ocean to the northeast of Taiwan Province. The south of North China was situated under the northwest edge of the subtropical high and an air flow convergence zone formed there. An NE-SW oriented shear line with an embedded meso-scale low extended from the north of Shanxi Province through Beijing Municipality into Liaoning Province at 850 hPa level, which moved southward over the next 12 hours. Furthermore, a surface cold front moved slowly from the north to the south. The above conditions worked together to provide favorable environmental conditions for the formation of the heavy rainfall.

3 Model and verification

3.1 Brief introduction of the numerical model and experimental design

The numerical model used in this study is the advanced regional prediction system (ARPS)[27] developed at the Center for Analysis and Prediction of Storms (CAPS), University of Oklahoma. It is a multi-scale non-hydrostatic compressible prediction system formulated in generalized terrain-following coordinates, which mainly focuses on meso-scale and storm-scale weather systems. In this study, the simulated domain is centered at (40.0°N, 115°E) and has 91×91 grids with a horizontal grid distance of 27 km. In the vertical, it consists of 43 sigma-z levels, with a minimum thickness layer of about 20 m near the surface and vertically stretched grids extending to model tops at height about 20 km. In the experiment, the full physics mode of ARPS is used, including a two-layer soil-vegetation model, 1.5 order TKE-based subgrid-scale turbulence, PBL parameterizations, Lin et al. (1983) ice microphysics, Kain-

Fritsch convective parameterization scheme, and full long- and short-wave radiation. A 24 h simulation was made, starting from the 1-degree NCEP global real-time analysis data at 00 UTC 12 August 2004, and using 6-hourly analyses from the same data set for lateral boundary conditions.

3.2 Verification of results

Fig. 1 shows the simulated 24 h accumulated rainfall and the corresponding observation. The simulation and the observation match very well except that the location of the simulated NE-SW oriented rainfall area is shifted a little to the south. The simulated first rainfall center is about 130 mm and the coverage of 100 mm is a little larger than the observed one. As to the other two simulated rainfall centers, one is 75 mm, which is a little smaller than the observed; and the other is quite similar to the observation.

Comparison of the 6 h accumulated rainfall between the simulations and the corresponding observations shows that the heavy rainfall was reproduced well by the model (Fig. 2). The simulated positions, timing and amounts of precipitation are all in good agreement with the observed ones. Therefore, the model can capture the evolution of weather systems and can reflect the activities of meso-scale convective systems.

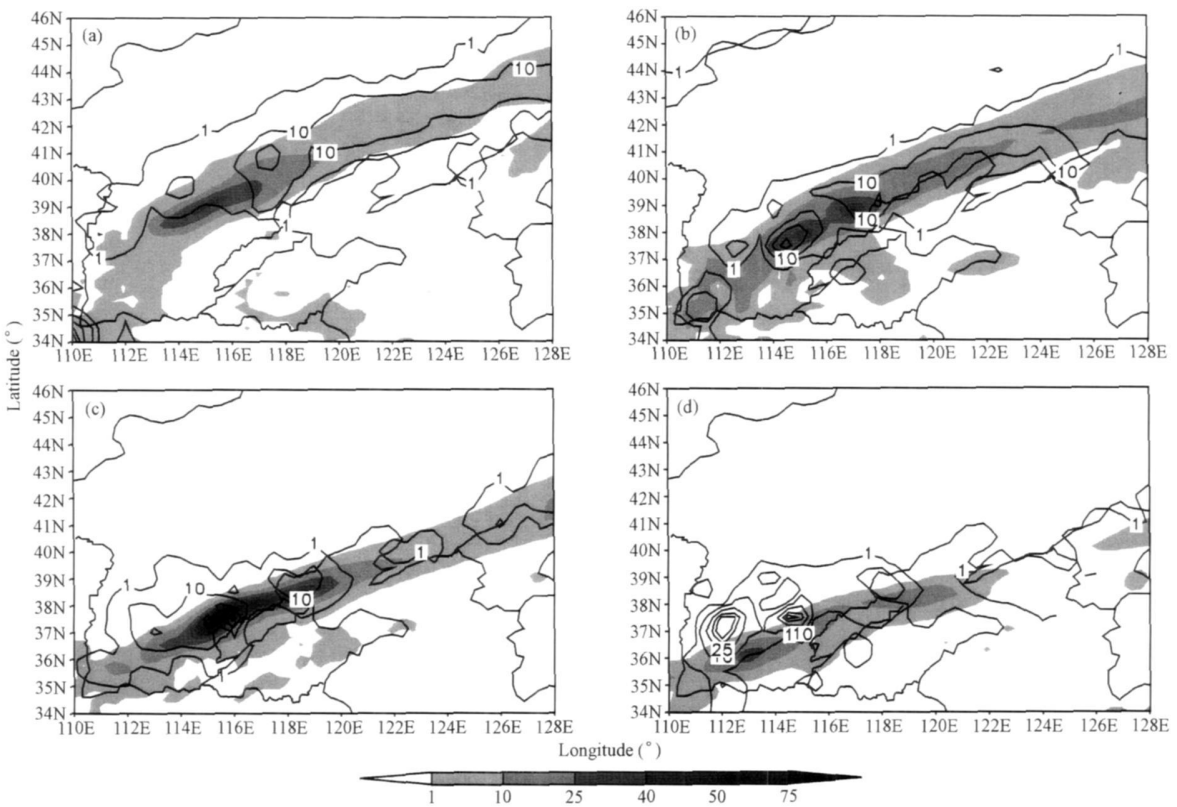

Fig. 2. Comparison between observed (solid line) and simulated (shaded) 6 h accumulated rainfall (units: mm). (a) 00-06UTC 12 August; (b) 06-12UTC 12 August; (c) 12-18UTC 12 August; (d) 18 UTC 12 August to 00 UTC 13 August (contours: 1, 10, 25, 40, 50, 75 mm).

From the comparison of the synoptic pattern (not shown), we can find that the typhoon, the westerly trough, the shear line at low levels and their evolutions were all simulated successfully by the ARPS model. The model did reproduce the heavy rainfall and further analysis will be carried out based on the simulated data.

4 Diagnostic analysis of the MVV

Although M_z is smaller than the horizontal components, Gao et al.[24,25] found that M_z is closely related with cloud hydrometeors and plays an important role in tropical convective activities. Therefore, the M_z is mainly discussed here.

4.1 Horizontal distribution of the vertical component of the MVV

Fig. 3 shows the distributions of the simulated M_z, the sum of mixing ratios of cloud hydrometeors and the vertical velocity at 04 UTC and 11 UTC August 12, respectively. It can be seen that a northeast-southwest oriented high values region of M_z with three main centers existed in North China at 850 hPa level at 04 UTC August 12 (Fig. 3(a)). It is interesting to see that the region of high M_z well corresponded with the sum of mixing ratios of cloud hydrometeors, which was also a region of upward motion providing favorable conditions for cloud development, and hence for rainfall (Fig. 3(c)). From hourly evolutions of the M_z and the sum of mixing ratios of cloud hydrometeors, the high values of the M_z matched to cloud hydrometeors as well as upward motion at all time (not shown). At 11 UTC 12 August, cloud hydrometeors moved southward and stretched westward, with the high values of M_z following the variation of cloud hydrometeors and agreeing well with the upward motion (Fig. 3(b), 3(d)). This clearly demonstrates that the shift and development of M_z is consistent with cloud hydrometeors.

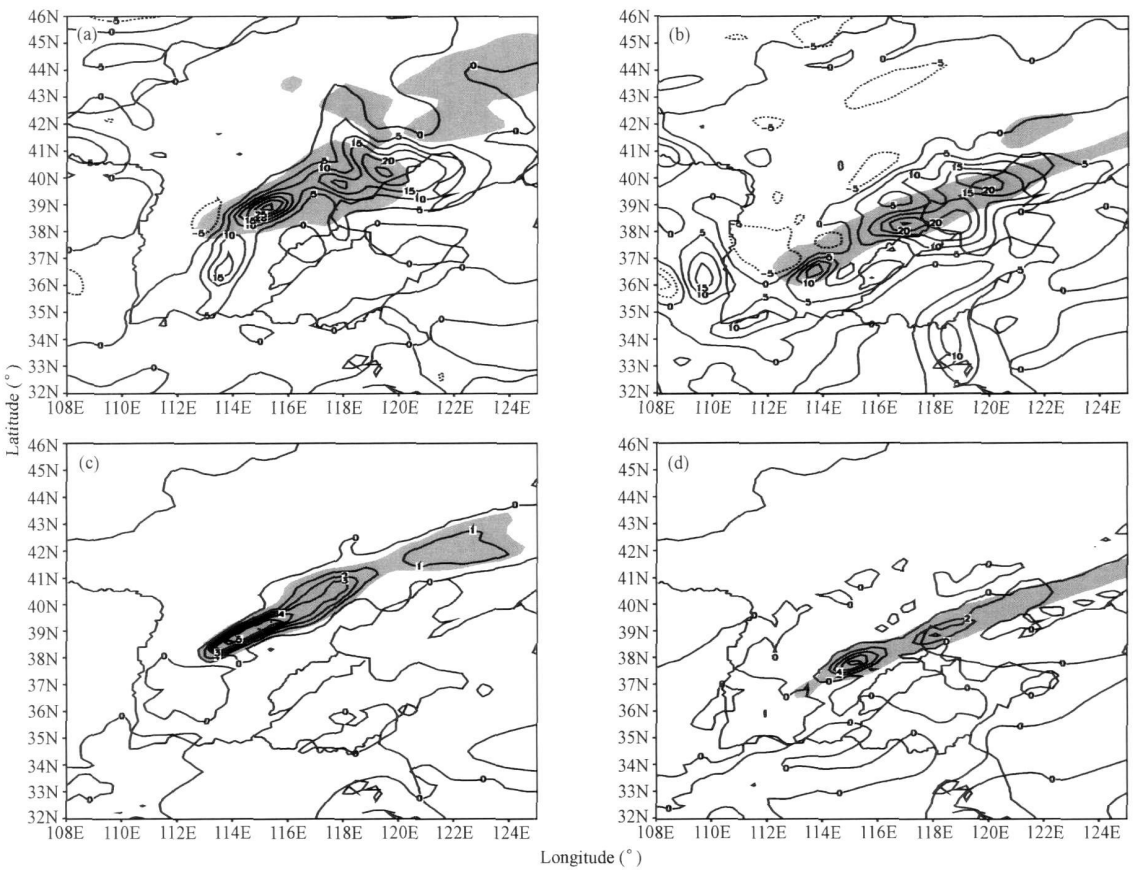

Fig. 3. Simulated M_z at 850 hPa (solid line in (a) and (b), unit: 10^{-11} m^2·s^{-1}·kg^{-1}), vertical velocity at 500 hPa (solid line in (c) and (d), unit: 10^{-2} m/s), and the sum of mixing ratios of cloud hydrometeors (shaded is lager than 1×10^{-1} g·kg^{-1}, (a) and (b) at 850 hPa, (c) and (d) at 500 hPa). (a) and (c) at 04UTC 12 August; (b) and (d) at 11 UTC 12 August.

4.2 Relationship between the mass-integrated vertical component of the MVV and cloud hydrometeors

From the above analyses, we can find that M_z is closely associated with cloud hydrometeors and upward motion, and so M_z can be regarded as a cloud-linked parameter. Then the mass-integrated M_z should have better relations with cloud hydrometeors and the rainfall. Therefore, the mass-integration of these variables will be discussed as follows.

Fig. 4 gives the distributions of the simulated mass-integrated M_z and the sum of mixing ratios of cloud hydrometeors at the same time covered in Fig. 3. Compared with Fig. 3, the M_z corresponded well with the cloud hydrometeors in Fig. 4. For example,

the distribution of M_z is more regular in Fig. 4(b), with only one main high value center rather than three centers in Fig. 3(b). Also, the M_z gradient significantly enhanced, with the high values of M_z corresponding better with the sum of the cloud hydrometeor mixing ratios. The cloud hydrometeors were mainly concentrated in the vicinity of high values of M_z and large M_z gradient. Because cloud hydrometeors directly associate with rainfall, the M_z should correspond with surface rainfall, which can be proved from Fig. 5. The distribution of the 6 h time-averaged and mass-integrated M_z (Fig. 5(a)) and the corresponding 6 h rain gauge observations (Fig. 5(b)) was very similar, indicating that M_z is strongly associated with the rain field.

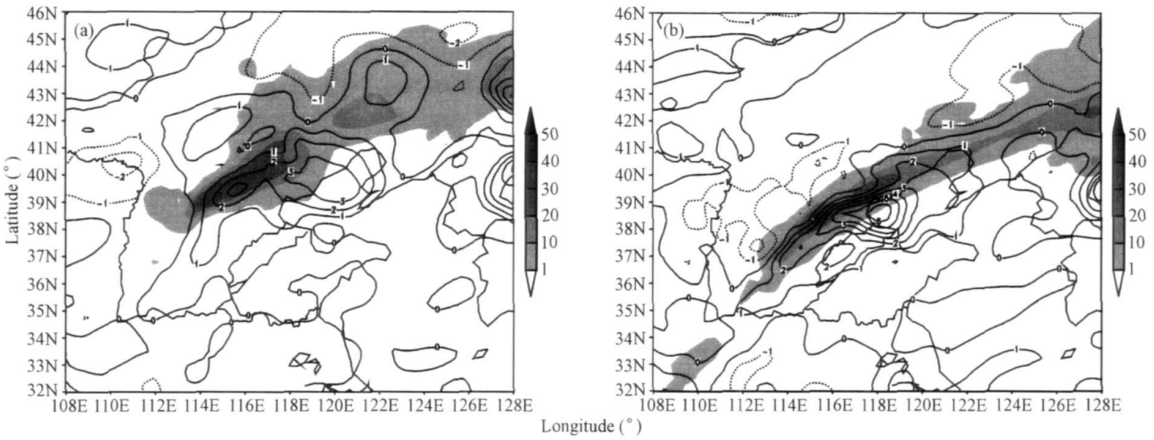

Fig. 4. Mass-integrated M_z (solid line, unit: $10^{-7}\,s^{-1}$) and the sum of mixing ratios of cloud hydrometeors (shaded, unit: $10^{-1}\,kg\cdot m^{-2}$). (a) 04 UTC 12 August; (b) 11 UTC 12 August.

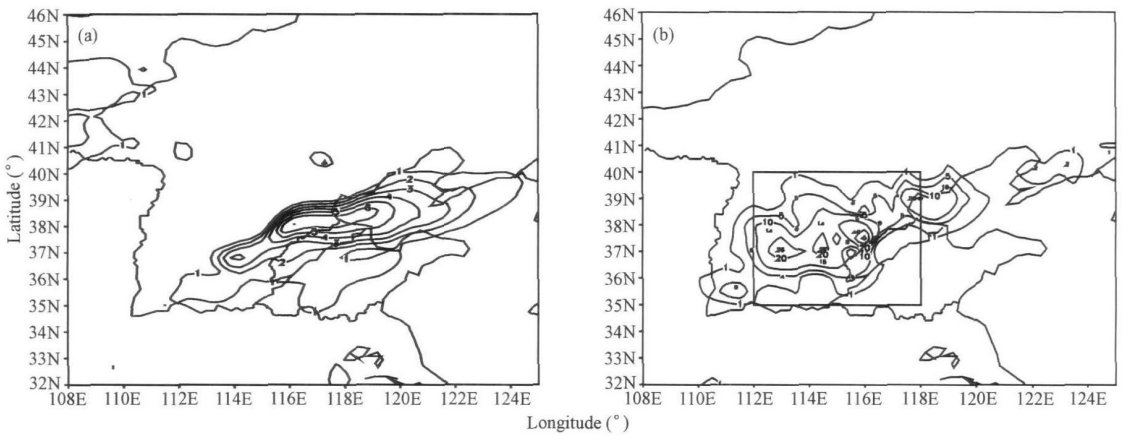

Fig. 5. Mass-integrated M_z ((a), unit: $10^{-7}\,s^{-1}$) and the corresponding observed rainfall ((b), unit: mm) from 12 UTC 12 August to 18 UTC 12 August.

To further illustrate the development and evolution relationship between M_z and surface rainfall, a time series of longitudinal cross-sections of [M_z] and the corresponding 1 h accumulated rainfall along 115.5°E was given. It can be seen that their distributions are very similar in time and space (Fig. 6). Both have two main high value centers, but the occurrence time of the high value centers is somewhat different. This can probably be attributed to the development of clouds and the rainfall not being completely in phase. As a matter of fact, clouds often develop prior to rainfall, which can explain why M_z is highly correlated with cloud hydrometeors but not completely in phase with clouds development. This suggests that M_z matches very well with surface rainfall during development and evolution processes of rainstorms.

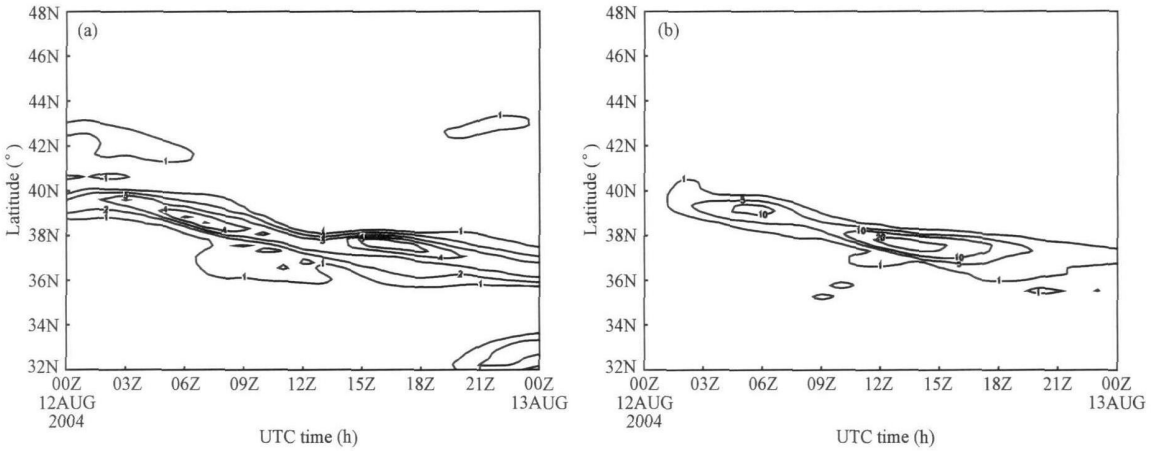

Fig. 6. Time series of longitudinal cross-sections of the M_z ((a), units: 10^{-11} m^2·s^{-1}·kg^{-1}) and the corresponding 1 h observed rainfall ((b), units: mm) along 115.5°E from 00 UTC 12 August to 00 UTC 13 August 200.

4.3 Quantitative relation between components of the MVV and cloud hydrometeors as well as precipitation rate

In order to further understand the relationships between components of the MVV and cloud hydrometeors as well as surface rainfall, the domain-mean and mass-integrated linear correlation coefficients between them were calculated. The domain was selected from 35 to 40°N, 112 to 118°E (the pane as shown in Fig. 5(b)), where rainfall mainly occurred. It can be seen that the figures of $[M_z]$ and $[q_c+q_r+q_i+q_s+q_h]$ are quite similar (Fig. 7(a)), with two peak values and one vale value respectively. Also, the peak values of cloud hydrometeors occurred earlier than M_z, which is in agreement with clouds usually developing before rainfall. The linear correlation coefficient between $[M_z]$ and $[q_c+q_r+q_i+q_s+q_h]$ is 0.95, at the 1% significance level, which shows that M_z is a parameter highly linked with clouds and can directly reflect the development and evolution of surface rainfall. The linear correlation coefficient between $[M_z]$ and the precipitation rate is 0.47, which also exceeds the 2% significance level. This further proves the above conclusion. $[M_x]$ is negative and its variation is out of phase with $[q_c+q_r+q_i+q_s+q_h]$, and $[M_y]$ is mainly positive. The correlation coefficient between $[M_x]$ and $[q_c+q_r+q_i+q_s+q_h]$ is only −0.39, and that between $[M_y]$ and $[q_c+q_r+q_i+q_s+q_h]$ is 0.41. Also, the variation of the precipitation rate with time is very similar to the variation of $[q_c+q_r+q_i+q_s+q_h]$, and their distributions are, on the whole, in phase (Fig. 7(b)), with their peak values and vale values occurring almost at the same time. Therefore, the M_z is highly correlated with cloud hydrometeors and can be used as a useful tool for tracing the development and evolution of rainfalls.

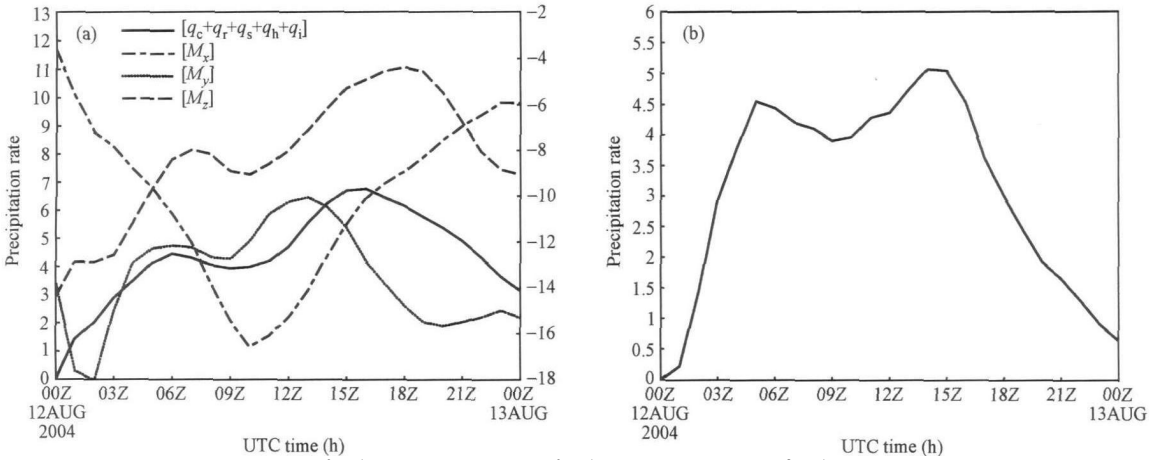

Fig. 7. Time series of $[M_x]$ (units: 10^{-6} s^{-1}), $[M_y]$ (units: 10^{-6} s^{-1}), $[M_z]$ (units: 10^{-8} s^{-1}) and $[q_c+q_r+q_i+q_s+q_h]$ (units: 10^{-1} kg·m^{-2}) (a) and precipitation rate (10^{-4} kg·m^{-2}s^{-1}) (b) over the area of 35—40°N, 112—118°E. (The abscissa is UTC time. In (a), the left axis labels $[M_z]$, $[M_y]$ and $[q_c+q_r+q_i+q_s+q_h]$, and the right axis labels $[M_x]$).

In addition, the linear correlation coefficient between [MPV] and [$q_c+q_r+q_i+q_s+q_h$] is 0.47, and that between [MPV] and precipitation rate is only −0.27, which is lower than that between M_z and cloud hydrometeors. Therefore, the M_z has some advantages in studying the rainfall area.

5 Physical meaning of the MVV

From the above analyses, we can find that M_z is strongly correlated with the rainfall area and may be a good indicator for tracing midlatitude convective rainstorms. A question then arises: why do they have such a good relation? The physical meaning of the MVV can help understand this, and so M_z will be discussed from its formula.

In Eq. (3c), M_z can be broken into two parts: $M_{z1}=\frac{1}{\rho}\left(\frac{\partial w}{\partial y}-\frac{\partial v}{\partial z}\right)\frac{\partial q_v}{\partial y}$ and $M_{z2}=-\frac{1}{\rho}\left[\left(\frac{\partial u}{\partial z}-\frac{\partial w}{\partial x}+f\right)\frac{\partial q_v}{\partial x}\right]$. Because vertical velocities are smaller than horizontal velocities and the horizontal scale is much larger than the vertical scale, the terms $\frac{\partial w}{\partial y}$ and $\frac{\partial w}{\partial x}$ are much smaller and can be neglected. Furthermore, f is about an order of magnitude smaller than $\left(\frac{\partial u}{\partial z}-\frac{\partial w}{\partial x}\right)$, and so it is neglected for discussion. M_{z1} may be written as $M_{z1}=-\frac{1}{\rho}\frac{\partial v}{\partial z}\frac{\partial q_v}{\partial y}$, where $\frac{\partial v}{\partial z}$ is the vertical shear of meridional wind associated with meridional secondary circulation and $\frac{\partial q_v}{\partial y}$ is the meridional gradient of specific humidity. Similarly, $M_{z2}=-\frac{1}{\rho}\frac{\partial u}{\partial z}\frac{\partial q_v}{\partial x}$, where $\frac{\partial u}{\partial z}$ is the vertical shear of zonal wind related with zonal secondary circulation and $\frac{\partial q_v}{\partial x}$ is the zonal gradient of specific humidity. Thus, the M_z is a new physical variable which couples horizontal wind vertical shear and the horizontal specific humidity gradient and synthetically reflects the variation of secondary circulation and the horizontal specific humidity gradient during the development of a system.

The secondary circulation is closely associated with vertical motion during the development of heavy rainfall, which is a direct cloud producer. This explains why M_z is strongly correlated with cloud hydrometeors. The secondary circulation is directly associated with the dynamic aspect of the convection, whereas the horizontal specific humidity gradients term is related with the thermodynamic aspect of the convection. Therefore, the M_z closely associates dynamic processes and thermodynamic processes with cloud microphysical processes. Although cloud formation and development are directly determined by cloud microphysical processes, the dynamic and thermodynamic processes determine cloud microphysical processes and play an indirect role in the evolution of convective systems. Thus, the M_z associates mesoscale dynamic and thermodynamic processes with cloud microphysical processes and can be used to reveal the occurrence and development of precipitation and then trace it.

6 Summary and discussion

In this study, the moist vorticity vector (MVV) has been applied to the study of a heavy rainfall event in North China with ARPS simulation data. In the 3D frame, the MVV has three components: zonal, meridional and vertical components. The regions of high values of the vertical component of the MVV match well with the rainfall.

The vertical component of the MVV represents the interaction between horizontal vorticity and the horizontal specific humidity gradient, which reflects the variation of secondary circulation and the horizontal specific humidity gradient during the developing processes of systems. Analysis of domain-mean and mass-integrated quantities showed that the correlation coefficient between the vertical component of the MVV and the sum of cloud hydrometeor mixing ratios was 0.95, which is significantly larger than that between cloud hydrometeors and the corresponding horizontal (zonal and meridional) components. The linear correlation coefficient between cloud hydrometeors and the vertical component of the MVV is larger than that between cloud hydrometeors and moist potential vorticity, which demonstrates that the vertical component of the MVV is a good indicator for midlatitude convective rainstorms and can provide a better tool for tracing the development and evolution of rainfall systems.

The results of this study have enlarged the potential application of the MVV. In the study of Gao et al.[24, 25], MVV was only used to study tropical

convective systems, and the performance of the MVV in the midlatitudes was not discussed. As known to all, convective systems in tropics and the midlatitudes are very different, for example, the vapor gradient is much more important than the temperature gradient because the atmosphere is unable to sustain a large temperature gradient in the tropics, whereas the temperature gradient is evident due to dry air associated with the cold frontal systems in the midlatitudes. In our study, North China is a semi-arid area, and the temperature gradient in the vicinity of the frontal systems is evident, but the vapor gradient is more important for the formation of the rainstorms. In fact, the contrast of dry air and moisture air is very evident in the vicinity of rainfall area due to continual moisture feeding and dry air associated with the cold frontal systems, and so the specific humidity gradient is very large. From the definition of the MVV, the MVV is related with vapor gradient and can grasp the significant difference between dry and moisture air cluster in rainfall area. Therefore, MVV has move advantages than MPV does in tracing rainfall in the midlatitudes.

A brief inspection of the 3D MVV is given in this paper, and its physical meaning and potential application in studying midlatitude convection are discussed. In future work, the vertical component of the MVV will be re-addressed in a more detailed context and will be applied to more cases and observational data.

Acknowledgements The authors would like to thank Dr. Xiaopeng Cui, Institute of Atmospheric Physics, Chinese Academy of Sciences, for his constructive comments on improving the manuscript significantly.

References

1 Ertel H. Ein neuer hydrodynamischer wirbelsatz. Meteorology Zeitschr Braunchweigs, 1942, 6: 277—281
2 Hoskins BJ, McIntyre ME and Robertson AW. On the use and significance of isentropic potential vorticity maps. Quart J Roy Meteor Soc, 1985, 111: 877—946
3 Cao Z and Cho H. Generation of moist vorticity in extratropical cyclones. J Atmos Sci, 1995, 52: 3263—3281
4 Cho H and Cao Z. Generation of moist vorticity in extratropical cyclones, part II: Sensitivity to moisture distribution. J Atmos Sci, 1998, 55: 595—610
5 Huo ZH, Zhang DL and Gyakum JR. Interaction of potential vorticity anomalies in extratropical cyclogenesis part I: Static piecewise inversion. Mon Wea Rev, 1999, 11: 2546—2561
6 Huo ZH, Zhang DL and Gyakum JR. Interaction of potential vorticity anomalies in extratropical cyclogenesis part II: Sensitivity to initial perturbations. Mon Wea Rev, 1999, 11: 2563—2575
7 Martin JE and Marsili N. Surface cyclolysis in the north Pacific ocean. Part II: Piecewise Potential vorticity diagnosis of a rapid cyclolysis event. Mon Wea Rev, 2002, 130: 1264—1281
8 Lackmann CM. Cold-frontal vorticity maxima, the low-level jet, and moisture transport in extratropical cyclones. Mon Wea Rev, 2002, 130: 59—74
9 Atallah EH and Bosart L. The extratropical transition and precipitation distribution of hurricane Floyd (1999). Mon Wea Rev, 2003, 131: 1063—1081
10 Bennetts DA andHoskins BJ. Conditional symmetric instability-A possible explanation for frontal rainbands. Q J Roy Meteor Soc, 1979, 105: 945—962
11 Wu GX, Cai YP and Tang XJ. Moist potential vorticity and slantwise vorticity development. Acta Meteorologica Sinica (in Chinese), 1995, 53(4): 387—404
12 Liu HZ and Zhang SQ. Moist potential vorticity and the three dimensional structure of a cold front with heavy rainfall. Journal of Applied Meteorology (in Chinese), 1996, 7(3): 275—283
13 Li Y and Duan X. Diagnostic analysis of moist potential vorticity for hail in southern yunnan. Journal of Applied Meteorology (in Chinese), 2000, 11(2): 242—247
14 Shou SW, Li YH and Fan K. Isentropic potential vorticity analysis of the mesoscale development in a heavy rain process. Acta Meteorologica Sinica (in Chinese), 2001, 59(5): 560—568
15 Cui XP, Wu GX and Gao ST. A numerical simulation and isentropic analysis of frontal cyclones over the Western Atlantic Ocean. Acta Meteorologica Sinica (in Chinese), 2002, 60: 385—399
16 Meng WG, Wang AY, Li JN, et al. Moist potential vorticity analysis of heavy rainfall and mesoscale convective systems in south China. Chinese Journal of Atmospheric Sciences (in Chinese), 2004, 28(3): 330—341
17 Bi BG, Liu YW and Li ZC. Numerical simulation extremely heavy rain in the southern shanxi province during 8—9 June 2002. Chinese Journal of Atmospheric Sciences (in Chinese), 2005, 29(5): 814—826
18 Gao ST, Lei T and Zhou YS. Moist potential vorticity anomaly with heat and mass forcings in torrential rain systems. Chin Phys Lett, 2002, 19(6): 878—880
19 Cui XP, Gao ST and Wu GX. Up-sliding slantwise vorticity development and the complete vorticity equation with mass forcing. Adv Atmos Sci, 2003, 20: 825—836
20 Cui XP, Gao ST and Wu GX. Moist potential vorticity and up-sliding slantwise vorticity development, Chin Phys Lett, 2003, 20: 167—169
21 Gao ST, Lei T, Zhou YS, et al. Dianostic analysis of moist potential vorticity anomaly in torrential rain systems. Journal of Applied Meteorology (in Chinese), 2002, 13(6): 662—670
22 Gao S, Wang X and Zhou Y. Generation of generalized moist potential vorticity in a frictionless and moist adiabatic flow. Geophys Res Lett, 2004, 31: L12113, doi: 10.1029/2003GL019152
23 Gao S, Ping F, Li X, et al. A convective vorticity vector associated with tropical convection: A two-dimensional cloud-resolving modeling study. J Geophys Res, 2004, 109: D14106, doi: 10.1029/2004JD004807
24 Gao S, Cui X, Zhou Y, et al. A modeling study of moist and dynamic vorticity vector associated with two-dimensional tropical convection. J Geophys Res, 2005, 110: D17104, doi: 10.1029/2004JD005675
25 Gao S, Li X, Tao W, et al. Convective and moist vorticity vectors associated with tropical oceanic convection: A three-dimensional cloud-resolving model simulation. J Geophys Res, 2007, 112: D01105, doi: 10.1029/2006JD007179
26 Cui XP, Gao ST and Li XF. Diagnostic analysis of mesoscale rainstorms in the Jiang-Huai valley of China with convection vorticity vector. Progress in Natural Science, 2007, 17(5): 559—568
27 Xue M, Droegemeier KK, Wong V, et al. ARPS Version 4.0 User's Guide. Center for Analysis and Prediction of Storms, University of Oklahoma, 1995. 380 pp (http://www.caps.ou.edu/ARPS/ARPS4.guide.html)